energies

MDPI

Article

Estimating the Subsurface Thermal Conductivity and Its Uncertainty for Shallow Geothermal Energy Use—A Workflow and Geoportal Based on Publicly Available Data

Elisa Heim [1,*], Marius Laska [2], Ralf Becker [2] and Norbert Klitzsch [1]

[1] Applied Geophysics and Geothermal Energy, RWTH Aachen University, Mathieustr. 30, 52074 Aachen, Germany; nklitzsch@eonerc.rwth-aachen.de
[2] Geodetic Institute and Chair for Computing in Civil Engineering & Geo Information Systems, RWTH Aachen University, Mies-van-der-Rohe-Str. 1, 52074 Aachen, Germany; marius.laska@gia.rwth-aachen.de (M.L.); ralf.becker@gia.rwth-aachen.de (R.B.)
* Correspondence: elisa.heim@eonerc.rwth-aachen.de

Abstract: Ground-source heat pumps with borehole heat exchangers (BHE) are an efficient and sustainable option to heat and cool buildings. The design and performance of BHEs strongly depend on the thermal conductivity of the subsurface. Thus, the first step in BHE planning is often assisted by a map representing the thermal conductivity of a region created from existing data. Such estimates have high uncertainty, which is rarely quantified. In addition, different methods for estimating thermal conductivity are used, for example, by the German federal states, resulting in incomparable estimates. To enable a consistent thermal conductivity estimation across state or country borders, we present a workflow for automatically estimating the thermal conductivity and its uncertainty up to user-defined BHE lengths. Two methods, which assess the thermal conductivity on different scales, are developed. Both methods are (1) based on subsurface data types which are publicly available as open-web services, and (2) account for thermal conductivity uncertainty by estimating its lowest, mean, and maximum values. The first method uses raster data, e.g., of surface geology and depth to groundwater table, and provides a large-scale estimate of the thermal conductivity, with high uncertainty. The second method improves the estimation for a small, user-defined target area by calculating the thermal conductivity based on the available borehole data in that area. The presented approach's novelty is a web-based geodata infrastructure that seamlessly connects data provision and calculation processes, with a geoportal as its central user interface. To demonstrate the approach, we use data from the federal state of Hamburg and compare the results of two target areas with the thermal conductivity estimation by the Geological Survey of Hamburg. Depending on the selected region, differences between the two estimates can be considerable (up to 1.2 $W\,m^{-1}\,K^{-1}$). The differences are primarily due to the selection of the thermal property database and the consideration of wet and dry rock. The results emphasize the importance of considering and communicating uncertainty in geothermal potential estimates.

Keywords: geothermal potential mapping; borehole heat exchanger; GSHP; thermal conductivity; uncertainty

Citation: Heim, E.; Laska, M.; Becker, R.; Klitzsch, N. Estimating the Subsurface Thermal Conductivity and Its Uncertainty for Shallow Geothermal Energy Use—A Workflow and Geoportal Based on Publicly Available Data. *Energies* **2022**, *15*, 3687. https://doi.org/10.3390/en15103687

Academic Editors: Javier F. Urchueguía and Borja Badenes

Received: 30 March 2022
Accepted: 9 May 2022
Published: 18 May 2022

1. Introduction

Fifty percent of the total energy consumption in Europe is used for heating and cooling applications [1], and in private households it is even more than seventy percent [2]. To date, fossil fuels still provide the majority of the thermal energy consumed [1]. An energy-efficient alternative for providing heat and cold with less emissions are ground-source heat pumps (GSHP) [3,4]. They employ the relatively constant temperature in the shallow subsurface, which is around 10–12 °C in Germany. This temperature level can be used for heating in combination with a heat pump and for direct cooling (free cooling). For extracting heat from the ground, different methods are used, such as closed-loop systems

or geothermal doublets. Most commonly, borehole heat exchangers (BHE) are used, which are closed pipes inserted vertically into the ground and through which a fluid circulates to extract heat from the subsurface.

The performance of BHEs depends on the ground heat exchange rate at site. The heat exchange rate, in turn, depends on operational and technical parameters of the GSHP system, as well as on the thermal properties of the subsurface [5]. When designing GSHPs, knowledge of the thermal properties is most important, because they determine if the amount of heat extracted by BHEs can be replenished by the rocks underground. Thereof, the thermal conductivity, i.e., the ability of a rock to conduct heat, is the most sensitive parameter for the BHE performance (e.g., [5–7]). The most precise estimate of thermal conductivity is obtained by conducting a thermal response test (TRT) within a borehole at site.

Because TRTs require drilling and are expensive, geothermal potential maps support the initial planning process of a geothermal installation. They hint towards the possible ground heat exchange rate at site. Because the term "geothermal potential" is not clearly defined [8], existing maps show various quantities, for example:

- subsurface parameters such as thermal conductivity and temperature [9–14],
- subsurface parameters combined with operational and technical parameters, for example the heat extraction rate [15–17], or the technical potential [18–26],
- subsurface, operational and technical parameters combined with the heating demand, resulting in the techno-economic potential [17,27–29].

Such geothermal potential maps have been created at various scales and with varying degrees of complexity. They are available, for example, on European scale [30,31], regional scale [16,32], and urban scale [8,33,34].

Despite the variety of geothermal potential maps, all approaches require an estimate of the thermal conductivity of the subsurface. This is commonly achieved by inferring the stratigraphic sequence a BHE would intersect using already available data, e.g., borehole databases and hydro-geological maps, and assigning thermal conductivities to the stratigraphic units. The values either come from laboratory measurements on samples taken in the study area [9,18,19,23,35] or published data compilations on these lithologies [21,22,36]. Literature values are, for example, given by the widely-used guidelines VDI4640 [37], ASHRAE [38] or other thermal conductivity databases [39].

We identify two issues with existing thermal conductivity estimation approaches. First, the calculation methods are tailored to the available subsurface data. This complicates both the application to other areas and the comparison of the geothermal potential of different regions. For example, in Germany, almost each of the 16 federal states has created its own geothermal potential map with a different methodology (Appendix A Table A1). Second, and more important, most of these studies disregard the considerable uncertainties involved in the estimation of the thermal conductivity based on existing data. Uncertainty mostly arises from assigning thermal conductivities to stratigraphic units [40]. This is because the effective thermal conductivity of a rock depends on the mineralogical composition, the porosity, and the water content [41–43]. In the subsurface, these parameters are heterogeneously distributed, which is why even thermal conductivity measurements on one rock type often show a huge spread [13,39,44]. Consequently, using one average thermal conductivity to represent an entire stratigraphic unit results in a high uncertainty. Because this uncertainty is not quantified, BHE fields are often over-sized and thus expensive. This is especially an issue for smaller BHE fields, where no TRT is carried out.

To overcome these issues, we present a methodology for predicting the effective thermal conductivity of the subsurface with quantified uncertainty. The method takes as input only publicly available and standardized hydro-geological and geological data types, to enable applicability to datasets of different regions, e.g., all German federal states. A web-based geodata infrastructure connects data provision, calculation processes and stores as well as provides calculation results, while a geoportal serves as user interface and

visualizes input data and results. This infrastructure automatizes the cumbersome step of geological data gathering for subsequent thermal-conductivity assessment and ensures that the data is always up to date. Methods for thermal conductivity estimation are introduced on two different scales. The first method is on a large scale, for example a federal state, and provides a first estimate of thermal conductivity. The second method updates the large-scale estimation in smaller target areas of particular interest, such as a small residential area. The focus of both methods lies on the consideration and communication of uncertainty in the assignment of thermal conductivity.

We demonstrate the approach using data from the federal state of Hamburg. However, it can be applied to all regions for which input data are publicly available. Finally, we compare our thermal conductivity estimates with thermal conductivity maps published by the federal state of Hamburg.

2. Data and Methods

In this chapter, we first provide an overview of the input data used to estimate thermal conductivity. We then explain the two methods for estimating the thermal conductivity and uncertainty, before introducing the geodata infrastructure.

2.1. Input Data

For estimating thermal properties, data containing information about the stratigraphy and water saturation in the subsurface are required, e.g., geological maps, borehole data, and hydrogeological data. Subsurface data is commonly available at different scales and at different authorities. In Germany, for example, state geological surveys are responsible for collecting and providing subsurface data. Both raw data, e.g., borehole data, and interpretations, such as geological maps, are available. Due to recent changes in the legal framework concerning geological data, this data is now publicly available (Geologiedatengesetz [45]). In combination with the ongoing process of digitalization, the law allows to design automatic workflows based on digital geological data. Here, we use six common subsurface data types (Table 1), which we group in four classes: borehole data, geological maps, elevation maps, and groundwater data.

Borehole databases are the most important input data type, because they are the only source of direct subsurface data. Containing lithologic descriptions along boreholes, they are required to assign thermal conductivities to petrographic units. The format of borehole databases is inconsistent throughout Germany, and different encoding standards are used (e.g., DABO, SEP3).

Geological maps are inferred from borehole data and mapping campaigns. They contain the distribution of geological units in 2-D at interfaces, most commonly the Earth's surface (surface geological map). Geological maps are also available for boundaries between structural units, for example, the quaternary base, which often corresponds to the base of unconsolidated rock (depth geological map). Both the surface geology and the depth geology help obtaining a large-scale estimate of thermal conductivity, especially in areas where borehole information is not available or the boreholes are not deep enough to cover the entire BHE length.

Elevation data are required to support the surface and depth geology with depth information. While the elevation of the Earth's surface is relatively certain, the depth of structural boundaries (quaternary base) is only inferred and thus more uncertain.

Groundwater data shows the depth from the surface to the groundwater table. Groundwater contour maps are derived from groundwater observation wells, oftentimes averaged over several years. The data allows to distinguish between the saturated and unsaturated zone. While the saturated zone is always wet, the unsaturated zone can contain seepage water, but is often dry. For simplicity, this study refers to the rock above the water table as dry and below as wet. The distinction is important because wet rock has a higher thermal conductivity than dry rock.

Except of borehole databases, all input data are cartographic data. Table 1 gives a summary of the input data. For demonstrating the thermal conductivity estimation approach, we use data from the federal state of Hamburg. Hamburg, a small German state, has made its geodata openly available online. Figure 1 shows the six input data types for Hamburg.

Table 1. Overview of input data.

Dataset	Description
Surface geology	distribution of petrographic units in 2-D at the Earth's surface (including loose rocks and soil deposits thicker than 1.5 m)
Depth geology	distribution of lithologic or petrographic units in 2-D at a characteristic boundary, oftentimes transition between loose and hard rock
Elevation model	relief at the Earth's surface
Quaternary base	often represents the relief at the interface between loose and hard rock
Depth to water table	average distance to water table
Borehole database	position, elevation and length of boreholes, and lithologic descriptions along borehole profiles

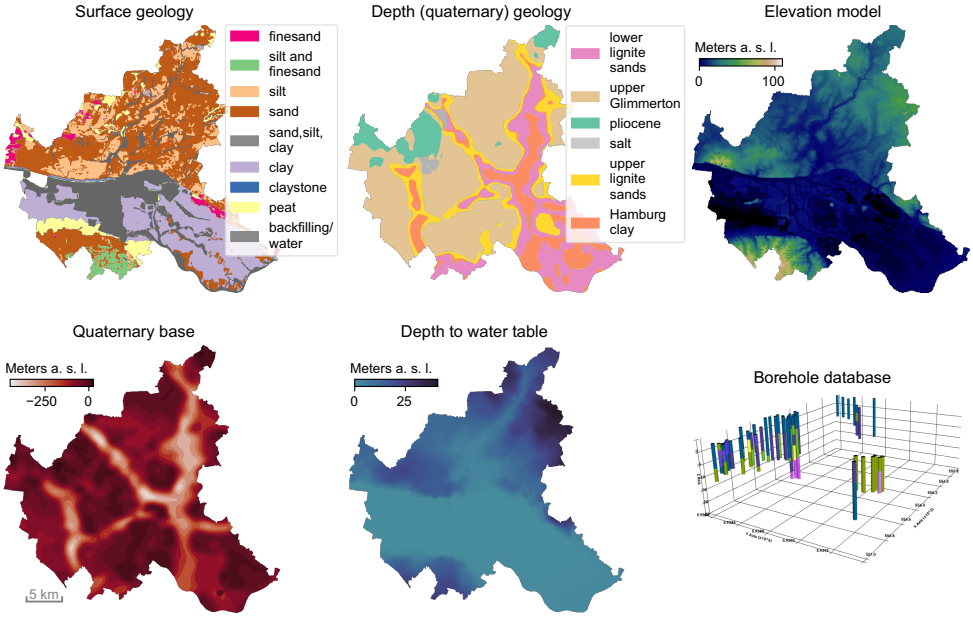

Figure 1. Visualization of the six input data types (Table 1) for the federal state of Hamburg. Borehole data is shown for a small sub-region only.

2.2. Methods for Estimating the Thermal Conductivity

We use two methods to estimate the average thermal conductivity of the subsurface, i.e., we estimate it on two different scales:

1. on a large scale with low resolution, which covers the entire study area (Hamburg) and uses 2-D data only,
2. on a small scale with high resolution, which additionally takes the borehole database as input.

Both approaches first infer the local stratigraphic sequence a BHE would intersect, which is described for the two methods in detail below. The stratigraphic sequence then gets assigned thermal properties. This is achieved with a thermal property mapper (TP mapper). The TP mapper links the petrographic descriptions given in the thematic maps and in the borehole database to thermal properties. It is a simple tree data structure with nodes for different lithologic IDs corresponding to different rock types. Every node has a collection of rock properties. For example, there are nodes for the thermal conductivity, the heat capacity, and the density. Nodes for other properties can easily be appended.

The TP mapper obtains its data from a thermal property database, in this study, the German guideline VDI 4640 sheet 1 [37]. It provides a collection of measurement-based values of thermal conductivity, heat capacity and density for 30 rock types, grouped by unconsolidated, sedimentary, magmatic and metamorphic rocks. For unconsolidated rocks, the VDI 4640 distinguishes between wet and dry rock, as here in particular the thermal properties depend on the water saturation. For every rock type and saturation, a recommended (mean), a minimal and maximal thermal conductivity are available. When the TP mapper is applied to a stratigraphic sequence, e.g., from a borehole interval, each interval is assigned three thermal conductivity values (mean, min., and max., Figure 2). The structure of the TP mapper allows for an easy addition or replacement of rock properties, for example, with other thermal property databases (e.g., [39]) or laboratory measurements.

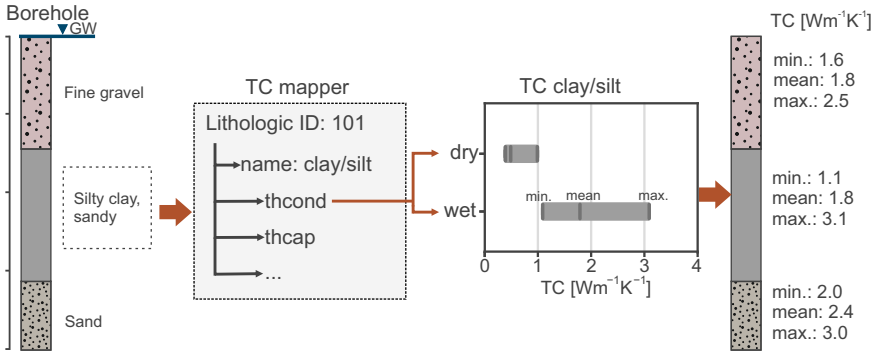

Figure 2. Translation of stratigraphic sequences to thermal conductivities. A petrographic term from a borehole interval is assigned to the closest lithologic ID in the TP mapper. Next, either wet or dry properties are assigned to the sequence, depending on the groundwater level.

2.2.1. Large-Scale TC Estimation

A large-scale estimate of the thermal conductivity in an area, e.g., for Hamburg, is obtained using the cartographic data only. The two geological maps (surface and depth geology) provide a large-scale overview of lithologies at the surface and the quaternary base. Assigning TC values to lithologies in geological maps is a simple and common method to obtain the TC distribution of larger areas (e.g., [31]). This approach is modified to use both geological maps as input. For that, the maps and their elevation data are combined in a plane model. This results in a pseudo-3-D model where the surface geology extends from the topography to the quaternary base, and the depth geology from the quaternary base to the BHE length (Figure 3). In regions with a deep Quaternary base, this leads to a thick sequence of pre-quaternary geology that is not realistic. Thus, we assume that the surface geology extends only to a depth of 15 m. Although the depth is arbitrarily chosen, it is considered a good compromise between accounting for surface geologic features on the one hand and avoiding unrealistically thick surface sediments on the other. After a depth of 15 m, we assign a mean value of all lithologic units at the surface as a background value. Next, the three units (surface geology, background geology, and depth geology) in the layer model are split into their "wet" and "dry" parts using the groundwater data (Figure 3). This allows the determination of the apparent thickness of each of the six units at every location on a 50 × 50 m raster covering the entire area of Hamburg. The apparent thickness at each location is input to the TP mapper, and the resulting thermal conductivities are weighted with the unit thickness, thus yielding the min., mean and max. thermal conductivity.

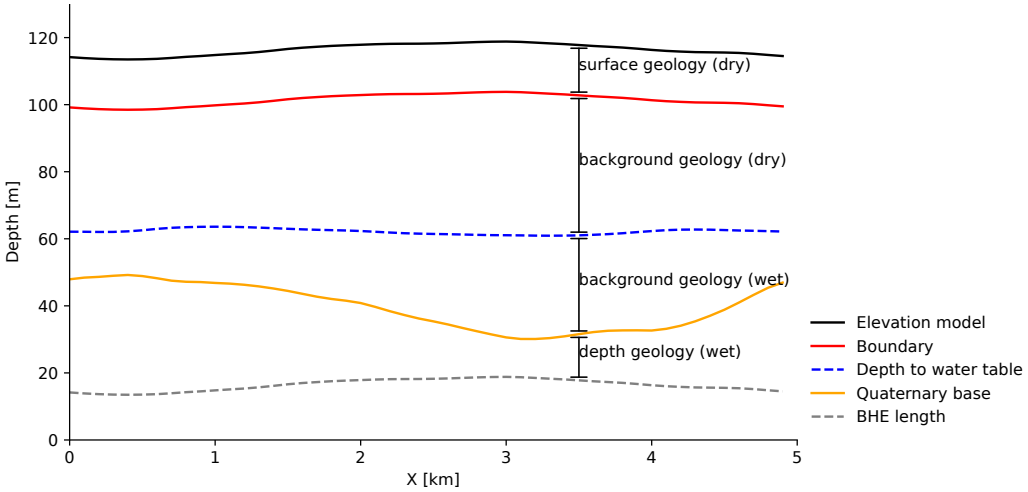

Figure 3. 2-D section trough a subset of the cartographic data to visualize the methodology used for the large-scale TC estimation.

2.2.2. High-Resolution TC Estimation in a User-Defined Target Area

Because the large-scale approach gives only a very coarse estimate, the high-resolution approach estimates the TC with higher resolution within a small, user-defined target area. This requires more computational effort, but gives the best possible prediction of TC for the target area by using the borehole database. The workflow starts with parsing the lithologic descriptions in the borehole data to map them to the closest lithologic ID in the TP mapper. Boreholes shorter than the BHE length are complemented by the model obtained from the cartographic data (Figure 4a). This results in a geological profile up to the BHE length (Figure 4b). In the profile, every borehole interval is assigned a wet or dry label using the groundwater data. Next, the profile is input for the TP mapper, which yields a thermal conductivity profile along the borehole (Figure 4c). Finally, the minimal, mean and maximal borehole thermal conductivity is calculated by thickness-weighting the thermal conductivity of each layer (Figure 4d). These steps are carried out for all boreholes within a target area.

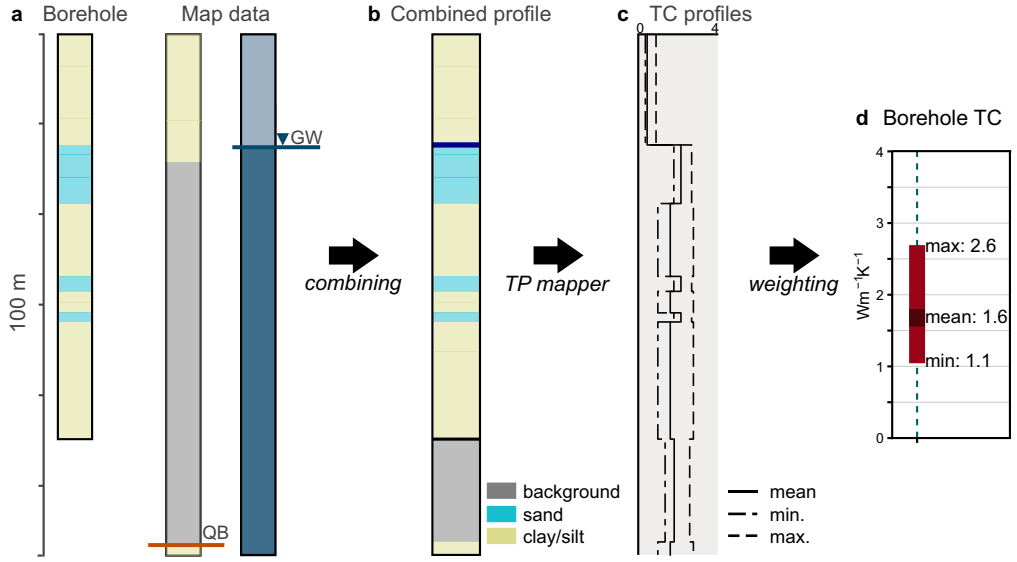

Figure 4. Estimation of the mean thermal conductivity of a borehole. Abbreviations: QB: Quaternary base, GW: groundwater level.

For visual results inspection, we extrapolate the borehole profiles in their vicinity by selecting a circular area around each borehole. The extrapolation's radius equals the

borehole length. Thus, the size of the circle reflects data coverage, because estimates from longer boreholes are more noticeable than those from shorter boreholes. Within each circle, the extrapolated borehole profile is supplemented with cartographic data from the surrounding area. The profiles within the circular area are input to the TP mapper, resulting in a min., mean and max. TC prediction in the vicinity of the boreholes. These values are written in grids with the extent of the target area and a resolution of 10×10 m. Because the boreholes are sorted by ascending length, values from longer boreholes overwrite values from shorter boreholes.

Result of the high-resolution approach is on the one hand the combined input data for the selected target area, and on the other hand the result of the TC prediction. The output grid is provided as a geotiff, while non-cartographic results are given as a PDF report. It contains information about the number and length of boreholes in the target area as well as visualizations of (1) the min., mean and max. thermal conductivity estimated around the boreholes, and (2) a comparison to the large-scale thermal conductivity estimate.

2.3. Web-Based Geodata Infrastructure

A geoportal respresents the central user interface of the web-based geodata infrastructure. Accessible in a webbrowser, it is meant for

1. data visualization,
2. data management and acquisition,
3. process management for high-resolution thermal conductivity estimations,
4. visual inspection of the results.

In the geoportal, the user can activate all available data sources (Table 1), e.g., borehole positions or the depth to groundwater, which are then superimposed on a base map (Figure 5). The geoportal is also responsible for initiating high-resolution thermal conductivity estimations. Further details on data and process management are given below.

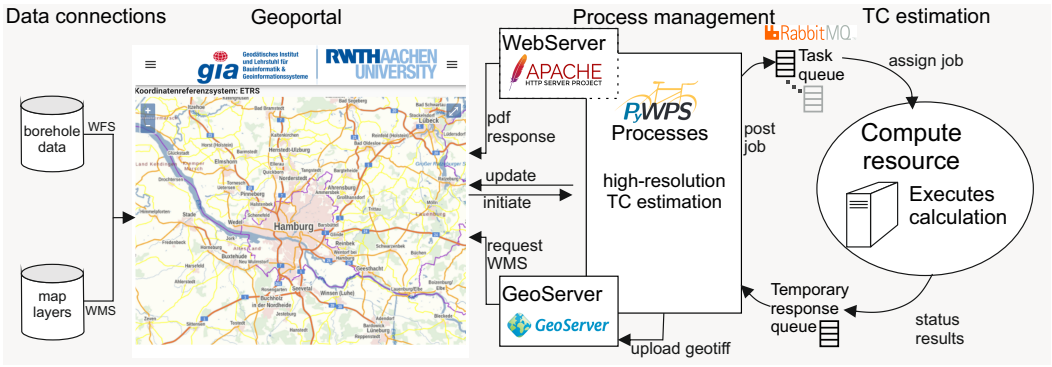

Figure 5. Overview of the web-based geodata infrastructure. Left: data connection to geodata servers, right: geodata infrastructure including asynchronous process communication.

2.3.1. Data Management

Both visualization and calculation processes access data directly from geodata servers through standardized web services, instead of storing the required data in a dedicated database. Interoperability is given due to well-defined interfaces of the Open Geospatial Consortium (OGC). The OGC provides several Open Web Services (OWS) that enable a standardized exchange of geospatial data via the World Wide Web. Cartographic data, such as geological maps, are visualized via Web Map Services (WMS), semantic data, such as borehole databases, are accessed via Web Feature Services (WFS) and geospatial processes are invoked by Web Processing Services (WPS). Accessing data directly using OWS ensures the highest possible level of data up-to-dateness.

2.3.2. Process Management

The user can initiate a high-resolution TC estimation from the geoportal. As the TC estimation can be costly in terms of resources, the task is mediated towards a dedicated computing resource. The architecture applied for this was proposed in [46] and rests on PyWPS [47] (implementation of the OGC WPS) as interface, RabbitMQ [48] as message broker to allow for realization of a remote procedure call pattern, and a GeoServer [49] instance to provide geospatial results via a WMS (Figure 5).

In the geoportal, the user can draw a target area, which is used as a boundary to access the data from the OWS. Furthermore, additional parameters can be submitted, such as the BHE length. When the user initiates the computation, the geoportal requests data within the target area from the geodata servers. Next, it constructs a WPS request, containing both user-defined input parameters and requested data. The WPS is forwarded to a server that operates the PyWPS. The task is then sent to a RabbitMQ message broker, which mediates it further to the processing unit where the high-resolution TC estimation takes place. Progress messages are communicated back via the message broker and stored at the PyWPS server so that the geoportal can request the process status.

Upon successful completion, both the geotiff containing the high-resolution mean thermal conductivity estimation and the PDF report are sent back to the PyWPS server via the message broker and are provided to the user in the geoportal. For that, the geotiff is uploaded to the GeoServer, which then allows for requesting the result as a map overlay via a WMS. The PDF report can be accessed from the geoportal via the internal Apache (https://httpd.apache.org/, accessed on 8 May 2022) webserver of the PyWPS.

3. Results

The large-scale and high-resolution TC prediction methods were applied using data from the federal state of Hamburg and results are shown for BHE lengths of 40 m and 100 m. The results are then compared to thermal conductivity maps published by the federal state of Hamburg [50], which will be referred to as $TC_{Hamburg}$. The maps of Hamburg were created based on a collection of laboratory measurements of the thermal conductivity of water-saturated core samples from the Hamburg area [50]. The measured thermal conductivities were assigned to boreholes deeper than 40 m and the resultant thermal conductivity profiles extrapolated in a structural model. By cropping the model at depths of 40, 60, 80, and 100 m, four maps were created, which are available as WMS (https://geodienste.hamburg.de/HH_WMS_Geothermie, accessed on 8 May 2022). We compare our results to the 40 m and 100 m maps, respectively.

First, we show the min., mean and max. TC map of the large-scale prediction for a BHE length of 100 m (TC_{ls}). Based on the comparison to $TC_{Hamburg}$, we identify two areas for the high-resolution thermal conductivity estimation ($TC_{high\text{-}res}$) and show the results in the second section.

3.1. Results of Large-Scale TC Prediction

The large-scale TC estimation workflow using data from Hamburg reveals the minimum, mean and maximum thermal conductivity up to a depth of 100 m (TC_{ls}, Figure 6A). The spatial distribution of thermal conductivity corresponds to characteristic boundaries in the cartographic data, e.g., boundaries of geological units in the surface geological map (compare Figure 1). Lowest thermal conductivity values are reached in the south, where the depth to water table is highest. The mean ($TC_{ls\text{-}mean}$) distributes around $(1.9 \pm 0.2)\,W\,m^{-1}\,K^{-1}$, the minimum ($TC_{ls\text{-}min}$) around $(1.4 \pm 0.2)\,W\,m^{-1}\,K^{-1}$, and the maximum ($TC_{ls\text{-}max}$) around $(2.8 \pm 0.2)\,W\,m^{-1}\,K^{-1}$ (Figure 6C).

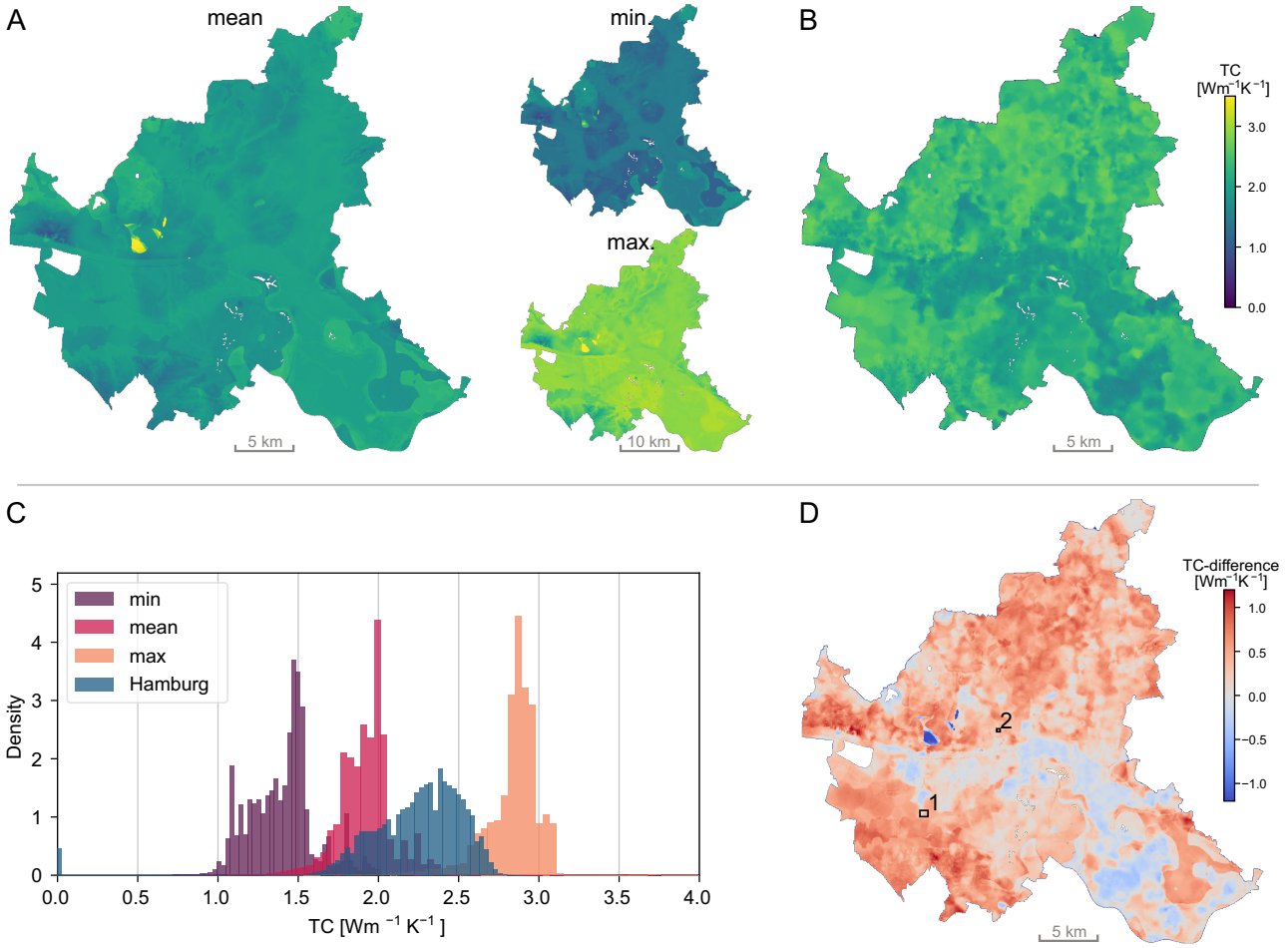

Figure 6. Thermal conductivity estimates for a BHE length of 100 m for the federal state of Hamburg. (**A**) result of the large-scale TC estimation, (**B**) TC map published by Hamburg, (**C**) histogram of TC values of the four maps, (**D**) difference between $TC_{Hamburg}$ and our mean estimate ($TC_{ls\text{-}mean}$) and location of target areas of the high-resolution approach.

$TC_{Hamburg}$ shows a different pattern than our TC prediction (Figure 6B). Instead of smooth shapes with anomalies, the map generally appears noisier. The mean TC lies with (2.20 ± 0.35) W m^{-1} K^{-1} between $TC_{ls\text{-}mean}$ and $TC_{ls\text{-}max}$ (Figure 6C).

The difference between $TC_{Hamburg}$ and $TC_{ls\text{-}mean}$ is shown in Figure 6D. While in the central part of Hamburg, TC_{ls} is higher than $TC_{Hamburg}$ (blue), it is lower in the outer areas (red). Nonetheless, in 96.9% of the area, $TC_{Hamburg}$ lies within the boundaries of our prediction, i.e., between our $TC_{ls\text{-}min}$ and $TC_{ls\text{-}max}$. In 1.6% of the area, $TC_{Hamburg}$ is higher than $TC_{ls\text{-}max}$ and in 1.5% of the area $TC_{Hamburg}$ is lower than $TC_{ls\text{-}min}$.

3.2. Results of High-Resolution TC Estimation for Specific Target Areas

We have chosen two regions and BHE lengths for the high-resolution TC estimation, which are marked in Figure 6D. Region 1 was chosen because of the high uncertainty of the large-scale estimate (more than 2 W m^{-1} K^{-1} for a BHE length of 100 m), and region 2 because of the high deviation to Hamburg of around 1.2 W m^{-1} K^{-1} for a BHE length of 40 m.

For both regions, the data (i.e., borehole intervals, depth to water table, quaternary base and geological maps) were requested from the geodata servers and combined in a 3-D block model for visualization and data quality control (Figure 7). Region 1 has an area of 0.37 km^2. Eleven boreholes are longer than 15 m, of which three cover the entire BHE length of 100 m. The groundwater level is right below the surface and the quaternary base is deeper than 100 m. Region 2 extends over an area of 0.08 km^2. Fifty-three boreholes

longer than 15 m are openly available. The groundwater table is around 10 m below the surface and the quaternary base at 30–40 m. Here, seven boreholes cover the entire BHE length of 40 m.

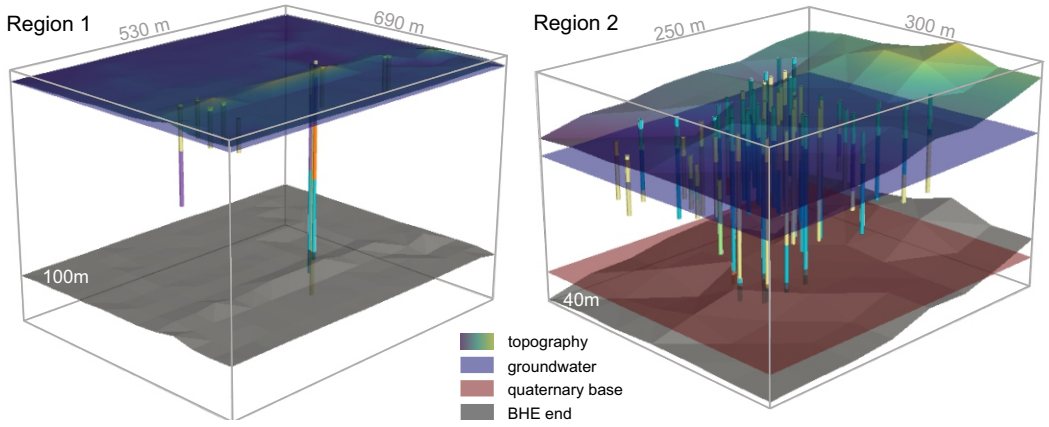

Figure 7. Input data for the two target regions, combined in a 3-D model. The legend of the borehole stratigraphies is shown in Figure 8.

Figure 8 shows for both regions the estimated min., mean and max. TC and the corresponding borehole stratigraphy and thermal conductivity profiles below. The boreholes are shown with ascending length. In **region 1,** seven boreholes are between 15 and 20 m long and thus do not cover the BHE length of 100 m. They were supplemented with the background value of the surface geology. For these boreholes, the spread between minimum and maximum TC is high, around 1.5 $W\,m^{-1}\,K^{-1}$. Towards longer boreholes, where detailed stratigraphic information is available for the entire BHE length, the spread between minimum and maximum decreases. The figure also shows the range and mean of the large-scale TC estimation at the borehole positions (A, in gray). With the high-resolution TC estimation, those mean values get updated towards a slightly higher thermal conductivity, while the range between minimum and maximum decreases. This way, the mean also moves closer to $TC_{Hamburg}$, which is shown as light-blue lines.

In **region 2**, (Figure 8), the groundwater level is shallower and more borehole data is available. Compared to TC_{ls}, the spread between minimum and maximum decreases, likewise to region 1. However, the mean gets only slightly updated towards higher values. Compared to $TC_{Hamburg}$, our mean is still significantly lower, and $TC_{Hamburg}$ is for some boreholes even higher than the maximal TC prediction of the high-resolution approach.

Besides these two regions, we studied additional target ares with different characteristics in regard to surface geology, depth geology, groundwater level and quaternary base, for BHE lengths of 40 and 100 m. The comparison to $TC_{large\text{-}scale}$ shows that oftentimes, the spread between minimum and maximum predicted TC is reduced, especially for long boreholes. However, this effect is less pronounced for complex borehole stratigraphies. Compared to $TC_{Hamburg}$, our mean TC is generally lower.

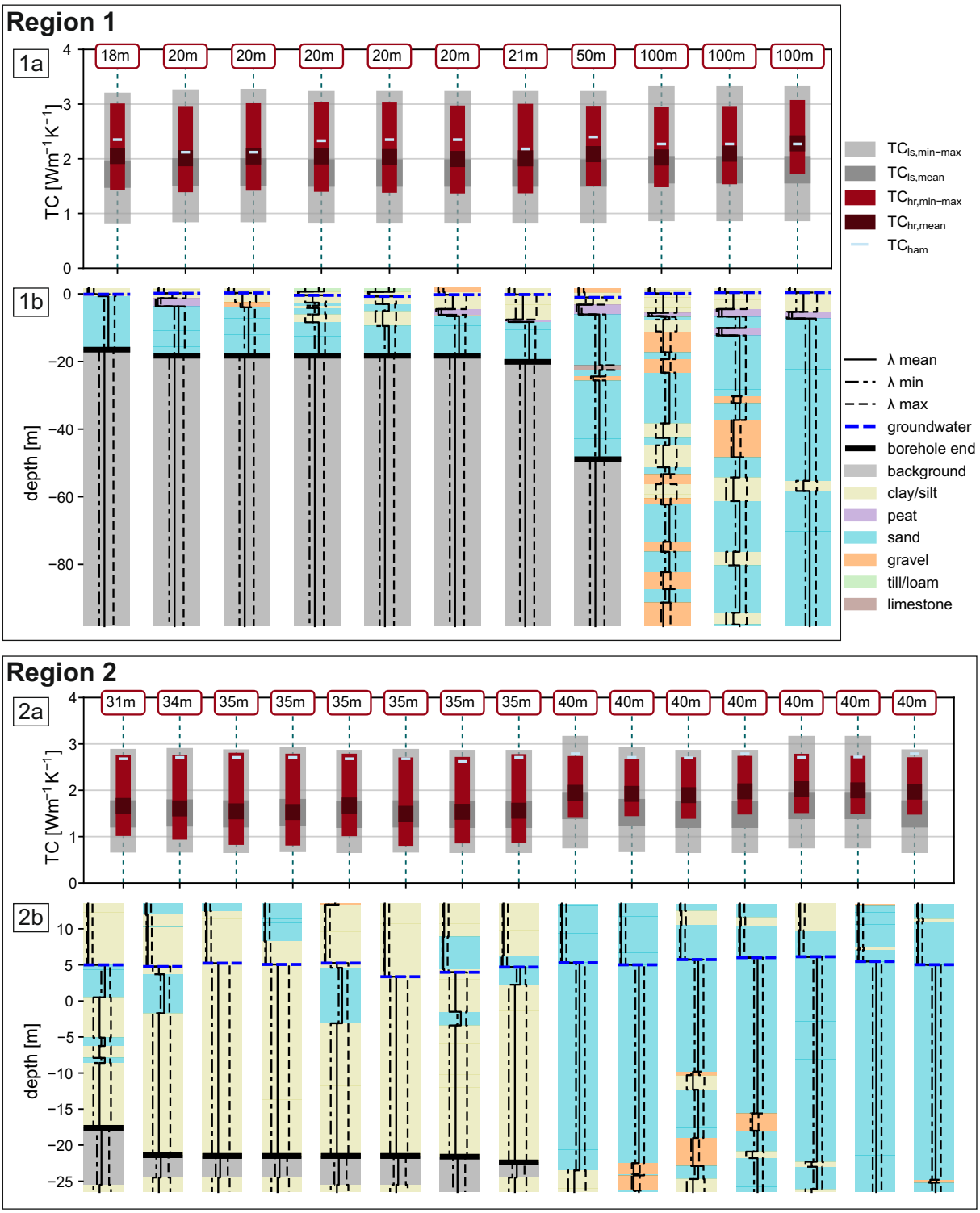

Figure 8. (**1a**,**2a**): Mean, min, and max TC value predicted at each borehole in region 1 (**top**) and region 2 (**bottom**) shown in red, and comparison to TC_{ls} (gray bars) and TC_{ham} as blue lines. (**1b**,**2b**): Corresponding borehole and TC profiles. The x-axis of the TC profiles ranges from 0 to 4 $W\,m^{-1}\,K^{-1}$. For visualization purposes, we show only the 15 longest of in total 53 boreholes in region 2.

4. Discussion

4.1. Discussion of Results

The results of the large-scale approach provide a first estimate of the mean thermal conductivity, with an oftentimes considerable spread of up to 2.5 $W\,m^{-1}\,K^{-1}$ between

the predicted minimal and maximal TC. When the water table is in the middle of the borehole, the spread is especially high. This is because when averaging the borehole TC, equal weight is given to the contrasting properties of wet and dry rock. The deviation to Hamburg is significant in some parts of the city, our mean lies partly below and partly above $TC_{Hamburg}$. In the central part it is often higher, while it is mostly lower in the peripheral areas. The cause of the discrepancy in the central part is probably that the quaternary base is deeper than 100 m and the water table is just below the surface (compare Figure 1). Thus, the outcome of our prediction depends solely on the surface geology. The discrepancy in the periphery is also due to the dependence of the approach on the geologic maps, because in contrast to the borehole data used in the Hamburg and high-resolution approach, the geological maps do not account for small-scale heterogeneity. As maps result from interpolation, they are subject to uncertainty themselves and do not reflect all variability of the subsurface. The strong dependence of TC on the geological maps is a major weakness of the large-scale approach, especially when the quaternary base is deep.

The high-resolution approach overcomes this issue by additionally taking the borehole data into account. Here, similar to the Hamburg approach, small-scale variations in the 3-D stratigraphy are considered. Consequently, the high-resolution approach brings our mean thermal conductivity estimate closer to $TC_{Hamburg}$. In addition, the spread between minimal and maximal predicted TC decreases. However, this observation can not be generalized, because the spread is dependent on the TC contrast of the lithologies and the depth of the groundwater.

Independent of the method, our mean thermal conductivity estimate is almost always lower than $TC_{Hamburg}$. The difference can be attributed to (1) the consideration of wet and dry rocks, and (2) to the mapped TC values. The depth of the water table, i.e., the water content, has a major impact on the effective thermal conductivity, especially in unconsolidated sediments [51,52]. For determining $TC_{Hamburg}$, only wet rock properties were mapped to the stratigraphic units [50], whereas the presented approach distinguishes between wet and dry rocks based on groundwater surface depth. This explains why the difference between $TC_{Hamburg}$ and $TC_{high\text{-}res}$ decreases with decreasing groundwater depth, as for example shown by region 1 and 2. Neglecting the possible occurrence of dry sediments is likely to overestimate the TC. However, the depth of the water table not always represents the boundary between water-saturated and unsaturated sediments. Both water retention and capillary rise can result in water saturation above the water table. Those effects are strongest in fine-grained sediments, i.e., clay and silt. Therefore, the approach could benefit from information on the water content of the unsaturated zone, e.g., by including maps of soil moisture. If this information is not available, a more realistic approach for estimating the subsurface TC might be to distinguish between dry and wet only for coarse sediments.

The consideration of dry rock is not the only reason for the difference between the thermal conductivities estimated by our high-resolution approach and $TC_{Hamburg}$. For example, in region 2, when considering all rocks as wet, the mean estimated thermal conductivity increases, but is still lower than $TC_{Hamburg}$. This is because of differences in the thermal conductivities assigned to the lithologic units. Figure 9 shows a comparison between the laboratory-measured thermal conductivities assigned for $TC_{Hamburg}$ and the VDI 4640 values used in our approach. The values for sand, gravel and silt/clay of the Hamburg database are considerable (up to 0.5 $W\,m^{-1}\,K^{-1}$) higher than the mean values of the VDI 4640. Moreover, the $TC_{Hamburg}$ database makes finer distinctions between different rock types compared to the VDI 4640. For example, instead of having one value for silt/clay in the VDI 4640, the Hamburg database has values for clay of different depositional ages and an additional value for silt. We discuss the selection of the thermal property database with more detail in the next section.

Another reason for differences is the availability of borehole data sets. Even though the "Geologiedatengesetz" was adopted in June 2020 [45], not all borehole data are available via OWS yet. This is on the one hand due to the ongoing process of digitization, and on the other hand due to reservation of ownership, meaning that the data owner must agree

to a transfer of data. Thus, the Hamburg maps are obtained from a larger database than our approach.

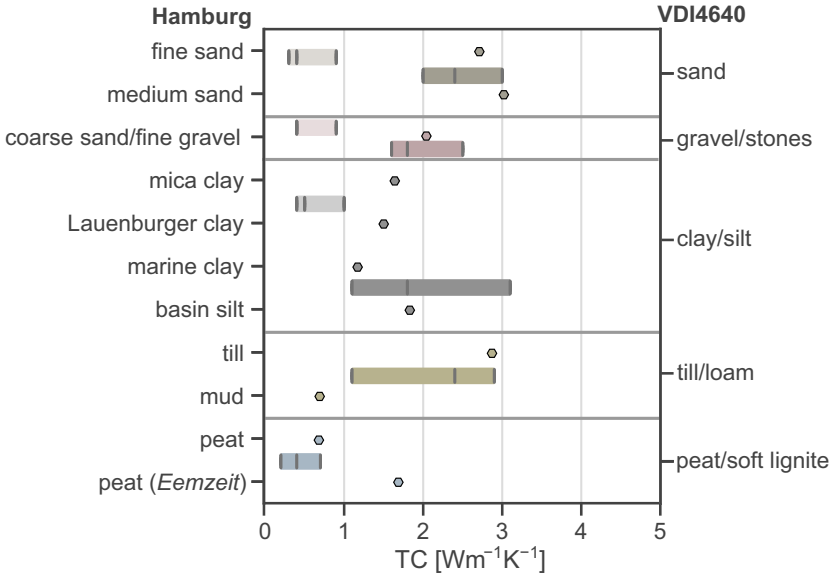

Figure 9. Comparison of laboratory measured thermal conductivity values in the Hamburg area [50] (dots) and corresponding min.-mean-max. ranges (bars) for both water-saturated (bright colors) and dry (pale colors) conditions from the VDI 4640 [37]. For till and peat, the VDI does not distinguish between saturated and dry conditions.

4.2. Challenges in Estimating the Thermal Conductivity from Existing Data

As seen in Section 4.1, the choice of the thermal property database has a major impact on the result. The selection of the TC database is a recently discussed issue with TC estimation procedures. It is oftentimes criticized to use generalized databases such as the VDI 4640, because of the huge spread of similar rock types from different regions [53]. This is why many authors rely on measurements taken on samples in the region of interest, for example [9,18,19,23,35]. Especially the VDI 4640, and its US-analogue, the ASHRAE [38], are criticized for not providing background information such as the measurement statistics, the measuring methods or the accuracy (e.g., [40]). Nonetheless, Ref. [18] has shown that there can be agreement between laboratory-measured values and general TC databases. This is why we believe that general databases such as the VDI 4640 are a good approximation as long as no more precise knowledge is available, given that the spread in TC is considered. This approach obtains its default TC values from the VDI 4640, but the flexible structure of the TP mapper allows for an easy updating with region-specific values.

Considering the spread of TCs also solves another major issue with the mapping of thermal properties. A single average thermal conductivity value for a rock can hardly account for the natural heterogeneity in the subsurface in terms of mineralogical composition and porosity [54,55]. Even if a laboratory-measured thermal conductivity of one sample of a lithologic unit was measured, the rocks nearby can have a different TC [56]. This also agrees with [53], who conducted laboratory-measurements on various samples of similar stratigraphies. They concluded that petrophysical properties can not be generalized on a regional scale. Because of the uncertainty in the TC due to heterogeneity and water saturation, we state that it is crucial to provide an accompanying estimate of uncertainty with the TC. The relevance of an uncertain TC for a GSHP-system is shown when calculating the temperature drop at the borehole wall using the Infinite Line Source (ILS) model by [57]. For example, for a minimum, mean and maximum TC of 1.9, 2.5, and 2.9 $\mathrm{W\,m^{-1}\,K^{-1}}$, and a constant heat extraction rate of 40 $\mathrm{W\,m^{-1}}$, the temperature change at the borehole wall after 200 h of heat extraction is −7.7, −5.8, and −5.0 K, respectively.

The uncertainty in thermal conductivity is not the only uncertainty affecting TC predictions, though it is the only uncertainty considered here. We have already discussed that all data types are subject to various uncertainties. In the raster data, these are, for example, simplifications, interpolation and their low resolution. Especially the groundwater level has a big influence on TC. Currently, both the large-scale and high-resolution approach use a constant groundwater level as input. This is only a momentary approximation of the real situation: The groundwater level can fluctuate in the range of several meters with seasons and years, thus affecting the TC estimate. For example, when the groundwater level is fluctuating in a layer of sand within 5 m, it affects the mean TC prediction of a 100 m borehole by 0.1 $W\,m^{-1}\,K$. Using a single value without this uncertainty can therefore result in an over- or under-prediction of thermal conductivity.

Moreover, groundwater flow has an important effect on the heat exchange potential of BHEs, because of the advective contribution to heat transfer. The approach presented here estimates only the conductive contribution to heat transfer, and the effective TC is likely to be underestimated if groundwater flow is present [40]. In environments with significant groundwater flow, we agree with [26], who recommend to conduct an in-situ thermal response test instead of assigning values from literature. We recommend to consult TC estimates based on existing data only for conduction-dominated settings.

Considering all known uncertainties in the input data, as discussed above, possibly leads to a very high uncertainty of the estimated TC. Nonetheless, we believe that communicating uncertainty is still advantageous in this case. It could hint towards unfavorable data availability or heterogeneous lithologies. A measure of the subsurface thermal conductivity with quantified uncertainty could then allow for better decision making in terms of geothermal investments, for example, because high uncertainty may initially motivate further investigation to reduce it.

5. Summary and Conclusions

This work was motivated by the missing comparability of different thermal conductivity estimation workflows, and the missing information about uncertainty. We present a workflow for automatically estimating the average thermal conductivity of the subsurface and its uncertainty up to a user-defined depth using common and publicly available data. The workflow was exemplary applied to data from the federal state of Hamburg, and thermal conductivity was estimated on two different scales. Results of the large-scale thermal conductivity prediction give a first indication, but show a high uncertainty. Hence, results from the large-scale approach should be considered as a first approximation only. With the high-resolution TC estimation using detailed borehole stratigraphy, the uncertainty can mostly be reduced and a more realistic TC is estimated. In addition, the overview of the available borehole stratigraphies within a target area can help users to assess the data quality.

However, we also observe significant differences compared to the TC estimate by the federal state of Hamburg. The selection of the thermal property database and the difference in considering dry and wet TC based on the groundwater level proved to be the main causes of discrepancies. Regarding thermal property databases, both region-specific and general databases fail to represent subsurface heterogeneity if only one single or average measurement value is used. Though region-specific databases might be more representative, it is most important to (1) use a statistically representative measurement collection of both wet and dry samples and (2) propagate the uncertainty of the statistics into the outcome, for example in the form of the standard deviation or min.-max. ranges. Besides the uncertainty in the thermal conductivity, other uncertainties such as groundwater flow or fluctuations in the groundwater level are also relevant and should be quantified in further work.

The structure of the proposed approach automatizes data aggregation and provides the data required for planning of BHEs on a detailed scale. This way, an expert user has the possibility to review the boreholes, for example, by excluding a borehole stratigraphy not fitting into the geological context. Another advantage is that the modular and automatic workflow can easily be extended to estimate other subsurface quantities, or applied to

datasets from other regions. The structure benefits from the recent developments regarding the availability and accessibility of geodata. The automatic combination of input data and method using web-based solutions will be beneficial for saving time, making subsurface predictions more comprehensible and reducing manual interpretation work.

Even though the high-resolution approach provides a good approximation of the subsurface thermal conductivity, the result possesses a high uncertainty. Moreover, it does not account for advective heat transfer by groundwater flow. Hence, results of TC estimation workflows can not replace a detailed assessment. For a more accurate estimation of thermal conductivity, a thermal response test is recommended. However, the developed web-based TC estimation provides a fast and comprehensive way of obtaining input data for e.g., site-selection or preliminary feasibility studies.

Possible Extensions and Outlook

This work can be improved and extended in several ways. The thermal property database (VDI 4640) could be replaced by a regional database of TC laboratory measurements like the one of Hamburg, which also provides standard deviations [50]. Another option is to link the approach to the *Petrophysical Property Database* of [58], an extensive measurement collection of various petrophysical properties.

Groundwater level fluctuations could be approximated by a uniform distribution instead of a fixed value. In regard to groundwater flow, we could estimate the thickness of known aquifers and their velocity using additional groundwater data and display the result in addition to the estimated thermal conductivity. Even though we do not expect to be able to quantify the convective component, we would give a qualitative estimation of its influence. In addition, we mentioned that the approach could benefit from a comparison to TRT data. Unfortunately, TRT data currently does not enter public databases, e.g., hosted by geological surveys. If TRT data were accessible to the public, TC estimation models could be validated and their uncertainty reduced, prior to any costly test drilling.

Besides these improvements, the result of the TC estimation method can be used for further studies. For example, the thermal conductivity estimate and its uncertainty can be used as input for estimating the technical potential, i.e., by taking technical and operational parameters of the ground-source heat pump system into account. Methods for this are for example the widely adopted G.POT algorithm introduced by [26] and used by, e.g., [18,19,22], or software solutions such as Earth Energy Designer [59] or GEO-HANDlight [60].

The web-based infrastructure for data and process management can be supplemented with additional data and processes to estimate other quantities, for example drillability, porosity, or thermal capacity. For this, the data infrastructure is built up modular resting on standardized open web services, so that further input data can be integrated effortlessly. This allows for extending the method to other areas, e.g., other German federal states or other countries.

Author Contributions: Conceptualization, E.H. and N.K.; methodology, E.H., M.L., R.B. and N.K.; software, R.B., M.L. and E.H.; validation, N.K. and E.H.; writing—original draft preparation, E.H. and M.L.; writing—review and editing, N.K. and R.B.; visualization, E.H. and M.L.; supervision, N.K.; project administration, N.K.; funding acquisition, N.K. All authors have read and agreed to the published version of the manuscript.

Funding: This manuscript was prepared based on research funded by E.ON, which we gratefully acknowledge. We are also grateful for the financial support by the Federal Ministry for Economic Affairs and Energy (BMWi), promotional reference 03ETW006A and 03ET1357A.

Institutional Review Board Statement: Not applicable.

Informed Consent Statement: Not applicable.

Data Availability Statement: All data from Hamburg is obtained from *Freie und Hansestadt Hamburg, Behörde für Umwelt und Energie* under the *Data licence Germany—attribution—Version 2.0* (licence text available at www.govdata.de/dl-de/by-2-0Data, accessed on 8 May 2022). The data can be found

at https://transparenz.hamburg.de (accessed on 15 February 2022). The python code for thermal conductivity estimation is available upon request.

Acknowledgments: We would like to thank the BUKEA Hamburg for their support in obtaining and understanding the data. Markus Bücherl is thanked for his constant feedback on the methodology. Gratitude is also expressed to colleagues who provided valuable comments and suggestions on the manuscript, and to student assistants who contributed to data analysis and code development.

Conflicts of Interest: The authors declare no conflict of interest.

Appendix A

Table A1. Overview of the information base on near-surface geothermal energy in the German federal states.

Federal State	Displayed Quantity
Baden Wurttemberg	Information System Near Surface Geothermal Energy for Baden Wurttemberg (ISONG): Maps of geothermal efficiency as a qualitative assessment in 4 levels (free of charge), specific heat extraction rate [W/m] to 40, 60, 80, 100m depth and for 1800 & 2400 h/a (fee required). Display of prognostic drilling profiles with information about drilling risks (karst, sulphates, aggressive groundwater).
Bavaria	UmweltAtlas Bayern: Site information on the average thermal conductivity [W/mK] to 20, 40, 60, 80, 100 m depth with 0.2 W/mK error range. Additional information about geological risks, water rights and hydrogeology.
Berlin	Umweltatlas Berlin: Maps of specific thermal conductivity [W/mK] and heat extraction rate [W/m] up to 40, 60, 80, 100 m depth and for 1800 and 2400 h/a (2017).
Brandenburg	Geothermieportal Brandenburg: Site query, thermal conductivity is estimated [W/mK] based on prognostic drilling profile with uncertainty information. Thermal conductivities based on VDI4640 & other literature values.
Bremen	Thermal conductivity map [W/mK] to 100 m depth.
Hamburg	Thermal conductivity [W/mK] to depth of 40, 60, 80, 100 m.
Hesse	Geothermie-Viewer Hessen: Thermal conductivity [W/mK] to depths of 40, 60, 80, 100 m. Assignment of thermal conductivities measured on samples from the Hesse area to drilling data and interpolation.
Mecklenburg Western Pomerania	Kartenportal Umwelt Mecklenburg Western Pomerania: Thermal conductivity [W/mK] up to 40, 60, 80, 100 m depth.
Lower Saxony	"Geothermie—geht das bei mir?" Estimation of required BHE meters, based energy consumption or house type and living space.
Northrhine Westphalia	Geothermieportal NRW: Geothermal yield for depths of 40, 60, 80, 100 m (free of charge), prognostic drilling profiles at any location (fee required).
Rhineland Palatinate	Thermal conductivity map for both dry & water-saturated rock. Classification of the permeability of the upper groundwater-conductor and groundwater-floor distance. Thermal conductivities for unconsolidated rocks taken from VDI 4640, for solid rocks obtained from the State Office for Geology and Mining.
Saarland	Map displaying ineligible, unfavorable and favorable areas for near-surface geothermal energy.
Saxony	Geothermieatlas Sachsen: maps of heat extraction [W/m] to depths of 40, 70, 100, 130 m and for heating durations of 1800 h and 2400 h.
Saxony-Anhalt	Maps displaying depth of bedrock, hydrogeology and non-geologic site criteria.
Schleswig Holstein	Geothermal planning map: Thermal conductivity up to depths of 50 and 100 m. Assignment of TC to boreholes based on a combination of VDI 4640, own measurements and the experience of neighboring states.
Thuringia	Geothermal information system: Thermal conductivity up to depths of 40, 60, 80, 100, 120 m. Allocation of TCs with consideration of groundwater level.

References

1. Heat Roadmap Europe. Heating and Cooling—Facts and Figures. 2017. Available online: https://www.isi.fraunhofer.de/content/dam/isi/dokumente/cce/2017/29882_Brochure_Heating-and-Cooling_web.pdf (accessed on 26 April 2022).
2. ODYSSEE-MURE. Declining Share of Space Heating in the EU | Space Heating | ODYSSEE-MURE. 2021. Available online: https://www.odyssee-mure.eu/publications/efficiency-by-sector/households/declining-share-space-heating-eu.html (accessed on 13 March 2022).
3. Connolly, D.; Lund, H.; Mathiesen, B.V.; Werner, S.; Möller, B.; Persson, U.; Boermans, T.; Trier, D.; Østergaard, P.A.; Nielsen, S. Heat Roadmap Europe: Combining District Heating with Heat Savings to Decarbonise the EU Energy System. *Energy Policy* **2014**, *65*, 475–489. [CrossRef]
4. Bayer, P.; Saner, D.; Bolay, S.; Rybach, L.; Blum, P. Greenhouse Gas Emission Savings of Ground Source Heat Pump Systems in Europe: A Review. *Renew. Sustain. Energy Rev.* **2012**, *16*, 1256–1267. [CrossRef]
5. Dehkordi, S.E.; Schincariol, R.A. Effect of Thermal-Hydrogeological and Borehole Heat Exchanger Properties on Performance and Impact of Vertical Closed-Loop Geothermal Heat Pump Systems. *Hydrogeol. J.* **2014**, *22*, 189–203. [CrossRef]
6. Han, C.; Yu, X.B. Sensitivity Analysis of a Vertical Geothermal Heat Pump System. *Appl. Energy* **2016**, *170*, 148–160. [CrossRef]
7. Vandenbohede, A.; Hermans, T.; Nguyen, F.; Lebbe, L. Shallow Heat Injection and Storage Experiment: Heat Transport Simulation and Sensitivity Analysis. *J. Hydrol.* **2011**, *409*, 262–272. [CrossRef]
8. Bayer, P.; Attard, G.; Blum, P.; Menberg, K. The Geothermal Potential of Cities. *Renew. Sustain. Energy Rev.* **2019**, *106*, 17–30. [CrossRef]
9. Janža, M.; Lapanje, A.; Šram, D.; Rajver, D.; Novak, M. Research of the Geological and Geothermal Conditions for the Assessment of the Shallow Geothermal Potential in the Area of Ljubljana, Slovenia. *Geologija* **2017**, *60*, 309–327. [CrossRef]
10. Di Sipio, E.; Galgaro, A.; Destro, E.; Teza, G.; Chiesa, S.; Giaretta, A.; Manzella, A. Subsurface Thermal Conductivity Assessment in Calabria (Southern Italy): A Regional Case Study. *Environ. Earth Sci.* **2014**, *72*, 1383–1401. [CrossRef]
11. Sakata, Y.; Katsura, T.; Nagano, K. Estimation of Ground Thermal Conductivity through Indicator Kriging: Nation-scale Application and Vertical Profile Analysis in Japan. *Geothermics* **2020**, *88*, 101881. [CrossRef]
12. Gerard, P.; Vincent, M.; François, B. A Methodology for Lithology-Based Thermal Conductivities at a Regional Scale for Shallow Geothermal Energy—Application to the Brussels-Capital Region. *Geothermics* **2021**, *95*, 102117. [CrossRef]
13. Luo, J.; Qiao, Y.; Xiang, W.; Rohn, J. Measurements and Analysis of the Thermal Properties of a Sedimentary Succession in Yangtze Plate in China. *Renew. Energy* **2020**, *147*, 2708–2723. [CrossRef]
14. García-Gil, A.; Vázquez-Suñe, E.; Alcaraz, M.M.; Juan, A.S.; Sánchez-Navarro, J.Á.; Montlleó, M.; Rodríguez, G.; Lao, J. GIS-supported Mapping of Low-Temperature Geothermal Potential Taking Groundwater Flow into Account. *Renew. Energy* **2015**, *77*, 268–278. [CrossRef]
15. De Filippis, G.; Margiotta, S.; Negri, S.; Giudici, M. The Geothermal Potential of the Underground of the Salento Peninsula (Southern Italy). *Environ. Earth Sci.* **2015**, *73*, 6733–6746. [CrossRef]
16. Ondreka, J.; Rüsgen, M.I.; Stober, I.; Czurda, K. GIS-supported Mapping of Shallow Geothermal Potential of Representative Areas in South-Western Germany—Possibilities and Limitations. *Renew. Energy* **2007**, *32*, 2186–2200. [CrossRef]
17. Schiel, K.; Baume, O.; Caruso, G.; Leopold, U. GIS-based Modelling of Shallow Geothermal Energy Potential for CO2 Emission Mitigation in Urban Areas. *Renew. Energy* **2016**, *86*, 1023–1036. [CrossRef]
18. Casasso, A.; Pestotnik, S.; Rajver, D.; Jež, J.; Prestor, J.; Sethi, R. Assessment and Mapping of the Closed-Loop Shallow Geothermal Potential in Cerkno (Slovenia). *Energy Procedia* **2017**, *125*, 335–344. [CrossRef]
19. Rajver, D.; Casasso, A.; Capodaglio, P.; Cartannaz, C.; Prestor, J.; Maragna, C.; Jez, J. Shallow Geothermal Potential with Borehole Heat Exchangers (BHEs): Three Case Studies in the Alps. In Proceedings of the World Geothermal Congress 2020+1, Reykjavik, Iceland, 24–27 October 2021; p. 13.
20. Ramos-Escudero, A.; García-Cascales, M.S.; Urchueguía, J.F. Evaluation of the Shallow Geothermal Potential for Heating and Cooling and Its Integration in the Socioeconomic Environment: A Case Study in the Region of Murcia, Spain. *Energies* **2021**, *14*, 5740. [CrossRef]
21. Previati, A.; Crosta, G.B. Regional-Scale Assessment of the Thermal Potential in a Shallow Alluvial Aquifer System in the Po Plain (Northern Italy). *Geothermics* **2021**, *90*, 101999. [CrossRef]
22. Taussi, M.; Borghi, W.; Gliaschera, M.; Renzulli, A. Defining the Shallow Geothermal Heat-Exchange Potential for a Lower Fluvial Plain of the Central Apennines: The Metauro Valley (Marche Region, Italy). *Energies* **2021**, *14*, 768. [CrossRef]
23. Santilano, A.; Donato, A.; Galgaro, A.; Montanari, D.; Menghini, A.; Viezzoli, A.; Di Sipio, E.; Destro, E.; Manzella, A. An Integrated 3D Approach to Assess the Geothermal Heat-Exchange Potential: The Case Study of Western Sicily (Southern Italy). *Renew. Energy* **2016**, *97*, 611–624. [CrossRef]
24. Galgaro, A.; Di Sipio, E.; Teza, G.; Destro, E.; De Carli, M.; Chiesa, S.; Zarrella, A.; Emmi, G.; Manzella, A. Empirical Modeling of Maps of Geo-Exchange Potential for Shallow Geothermal Energy at Regional Scale. *Geothermics* **2015**, *57*, 173–184. [CrossRef]
25. Viesi, D.; Galgaro, A.; Visintainer, P.; Crema, L. GIS-supported Evaluation and Mapping of the Geo-Exchange Potential for Vertical Closed-Loop Systems in an Alpine Valley, the Case Study of Adige Valley (Italy). *Geothermics* **2018**, *71*, 70–87. [CrossRef]
26. Casasso, A.; Sethi, R. G.POT: A Quantitative Method for the Assessment and Mapping of the Shallow Geothermal Potential. *Energy* **2016**, *106*, 765–773. [CrossRef]

27. Gemelli, A.; Mancini, A.; Longhi, S. GIS-based Energy-Economic Model of Low Temperature Geothermal Resources: A Case Study in the Italian Marche Region. *Renew. Energy* **2011**, *36*, 2474–2483. [CrossRef]
28. Perego, R.; Pera, S.; Galgaro, A. Techno-Economic Mapping for the Improvement of Shallow Geothermal Management in Southern Switzerland. *Energies* **2019**, *12*, 279. [CrossRef]
29. Tissen, C.; Menberg, K.; Benz, S.A.; Bayer, P.; Steiner, C.; Götzl, G.; Blum, P. Identifying Key Locations for Shallow Geothermal Use in Vienna. *Renew. Energy* **2021**, *167*, 1–19. [CrossRef]
30. Bertermann, D.; Klug, H.; Morper-Busch, L. A Pan-European Planning Basis for Estimating the Very Shallow Geothermal Energy Potentials. *Renew. Energy* **2015**, *75*, 335–347. [CrossRef]
31. Ramos-Escudero, A.; García-Cascales, M.S.; Cuevas, J.M.; Sanner, B.; Urchueguía, J.F. Spatial Analysis of Indicators Affecting the Exploitation of Shallow Geothermal Energy at European Scale. *Renew. Energy* **2021**, *167*, 266–281. [CrossRef]
32. Götzl, G.; Ostermann, V.; Kalasek, R.; Heimrath, R.; Steckler, P.; Zottl, A.; Novak, A.; Haindlmaier, G.; Hackl, R.; Shadlau, S.; et al. GEO-Pot: Seichtes Geothermie Potenzial Österreichs. Überregionale, Interdisziplinäre Potenzialstudie Zur Erhebung Und Darstellung Des Oberflächennahen Geothermischen Anwendungspotenzials Auf Grundlage Eines Regelmäßigen Bearbeitungsrasters. *Österreichische Wasser-und Abfallwirtsch.* **2010**, *62*, 5–6. [CrossRef]
33. Miglani, S.; Orehounig, K.; Carmeliet, J. A Methodology to Calculate Long-Term Shallow Geothermal Energy Potential for an Urban Neighbourhood. *Energy Build.* **2018**, *159*, 462–473. [CrossRef]
34. Zhu, K.; Blum, P.; Ferguson, G.; Balke, K.D.; Bayer, P. The Geothermal Potential of Urban Heat Islands. *Environ. Res. Lett.* **2010**, *5*, 044002. [CrossRef]
35. Georgina, A.; Roger, V.; Alessandro, C.; Ignasi, H.; Jessica, A.; Marc, P. Assessment of Closed-Loop Shallow Geothermal Potential in Catalonia Using GIS Tools. In Proceedings of the European Geothermal Congress, Hague, The Netherlands, 11–14 June 2019; p. 8.
36. Kahnt, D.R. *Potenzialstudie zur Nutzung der geothermischen Ressourcen des Landes Berlin (Modul 2)-Abschlussbericht*; Abschlussbericht zu den Ergebnissen; GEOS Ingenieurgesellschaft: Halsbrücke, Germany, 2011; p. 67.
37. VDI-Fachbereich Energietechnik. *VDI 4640 Blatt 1—Thermische Nutzung des Untergrunds-Grundlagen, Genehmigungen, Umweltaspekte*; Part 1: Thermal Use of the Underground—Fundamentals, Approvals, Environmental Aspects; Verein Deutscher Ingenieure: Alexisbad, Germany, 2010.
38. American; Society of Heating, Refrigerating and Air-Conditioning Engineers. ASHRAE Handbook: HVAC Applications—Geothermal Energy. In *Heating, Ventilating and Air-Conditioning Applications, SI ed.*; ASHRAE: Atlanta, GA, USA, 2011.
39. Dalla Santa, G.; Galgaro, A.; Sassi, R.; Cultrera, M.; Scotton, P.; Mueller, J.; Bertermann, D.; Mendrinos, D.; Pasquali, R.; Perego, R.; et al. An Updated Ground Thermal Properties Database for GSHP Applications. *Geothermics* **2020**, *85*, 101758. [CrossRef]
40. Galgaro, A.; Dalla Santa, G.; Zarrella, A. First Italian TRT Database and Significance of the Geological Setting Evaluation in Borehole Heat Exchanger Sizing. *Geothermics* **2021**, *94*, 102098. [CrossRef]
41. Brigaud, F.; Vasseur, G. Mineralogy, Porosity and Fluid Control on Thermal Conductivity of Sedimentary Rocks. *Geophys. J. Int.* **1989**, *98*, 525–542. [CrossRef]
42. Beier, R.A.; Smith, M.D.; Spitler, J.D. Reference Data Sets for Vertical Borehole Ground Heat Exchanger Models and Thermal Response Test Analysis. *Geothermics* **2011**, *40*, 79–85. [CrossRef]
43. Gehlin, S.E.A.; Hellström, G. Influence on Thermal Response Test by Groundwater Flow in Vertical Fractures in Hard Rock. *Renew. Energy* **2003**, *28*, 2221–2238. [CrossRef]
44. Jorand, R.; Clauser, C.; Marquart, G.; Pechnig, R. Statistically Reliable Petrophysical Properties of Potential Reservoir Rocks for Geothermal Energy Use and Their Relation to Lithostratigraphy and Rock Composition: The NE Rhenish Massif and the Lower Rhine Embayment (Germany). *Geothermics* **2015**, *53*, 413–428. [CrossRef]
45. Geologiedatengesetz. *Gesetz zur staatlichen Geologischen Landesaufnahme sowie zur Übermittlung, Sicherung und öffentlichen Bereitstellung Geologischer Daten und zur Zurverfügungstellung Geologischer Daten zur Erfüllung öffentlicher Aufgaben (Geologiedatengesetz–GeoIDG)*, 19 June 2020.
46. Laska, M.; Herle, S.; Blankenbach, J.; Fichter, E.; Frisch, J. WhizPS: An Architecture for Well-Conditioned, Scalable Geoprocessing Services Based on the WPS Standard. In Proceedings of the GEOProcessing 2019: The Eleventh International Conference on Advanced Geographic Information Systems, Applications, and Services, Athens, Greece, 24–28 February 2019.
47. PyWPS Development Team. Python Web Processing Service (PyWPS). 2009. Available online: https://pywps.org (accessed on 26 April 2022).
48. RabbitMQ. Available online: https://www.rabbitmq.com/ (accessed on 22 April 2022).
49. GeoServer. Available online: http://geoserver.org/ (accessed on 22 April 2022).
50. Behörde für Umwelt, Klima, Energie und Agrarwirtschaft Hamburg. *Leitfaden Erdwärmenutzung*; Behörde für Umwelt, Klima, Energie und Agrarwirtschaft Hamburg: Hamburg, Germany, 2021; p. 44.
51. Sipio, E.D.; Bertermann, D. Thermal Properties Variations in Unconsolidated Material for Very Shallow Geothermal Application (ITER Project). *Int. Agrophys.* **2018**, *32*, 149–164. [CrossRef]
52. Luo, J.; Luo, Z.; Xie, J.; Xia, D.; Huang, W.; Shao, H.; Xiang, W.; Rohn, J. Investigation of Shallow Geothermal Potentials for Different Types of Ground Source Heat Pump Systems (GSHP) of Wuhan City in China. *Renew. Energy* **2018**, *118*, 230–244. [CrossRef]
53. Hartmann, A.; Pechnig, R.; Clauser, C. Petrophysical Analysis of Regional-Scale Thermal Properties for Improved Simulations of Geothermal Installations and Basin-Scale Heat and Fluid Flow. *Int. J. Earth Sci.* **2008**, *97*, 421–433. [CrossRef]

54. Albert, K.; Schulze, M.; Franz, C.; Koenigsdorff, R.; Zosseder, K. Thermal Conductivity Estimation Model Considering the Effect of Water Saturation Explaining the Heterogeneity of Rock Thermal Conductivity. *Geothermics* **2017**, *66*, 1–12. [CrossRef]
55. Jorand, R.; Vogt, C.; Marquart, G.; Clauser, C. Effective Thermal Conductivity of Heterogeneous Rocks from Laboratory Experiments and Numerical Modeling. *J. Geophys. Res. Solid Earth* **2013**, *118*, 5225–5235. [CrossRef]
56. Jia, G.S.; Tao, Z.Y.; Meng, X.Z.; Ma, C.F.; Chai, J.C.; Jin, L.W. Review of Effective Thermal Conductivity Models of Rock-Soil for Geothermal Energy Applications. *Geothermics* **2019**, *77*, 1–11. [CrossRef]
57. Carslaw, H.S.; Jaeger, J.C. *Conduction of Heat in Solids*, 2nd ed.; Clarendon Press: Oxford, UK; Oxford University Press: New York, NY, USA, 1986.
58. Bär, K.; Reinsch, T.; Bott, J. The PetroPhysical Property Database—A Global Compilation of Lab-Measured Rock Properties. *Earth Syst. Sci. Data* **2020**, *12*, 2485–2515. [CrossRef]
59. Hellström, G.; Sanner, B. Software for Dimensioning of Deep Boreholes for Heat Extraction. *Proc. Calorstock* **1994**, *94*, 195–202.
60. Königsdorff, R.; Veser, S. GEO-HANDlight, Computerprogramm Zur Berechnung Der Auslegung von Erdwärmesonden Für Heiz-und Kühlzwecke. Hochschule Biberach, University of Applied Sciences, Institute of Building & Energy Systems, Germany. 2008. Available online: https://innosued.de/energie/geothermie-software-2/ (accessed on 26 April 2022).